Ultrafast charge transfer in a type-II MoS_2-$ReSe_2$ van der Waals heterostructure

LU ZHANG,[1] DAWEI HE,[1] JIAQI HE,[1,*] YANG FU,[1] ANG BIAN,[1] XIUXIU HAN,[1] SHUANGYAN LIU,[1] YONGSHENG WANG,[1,*] AND HUI ZHAO[2]

[1]*Key Laboratory of Luminescence and Optical Information, Ministry of education, Institute of Optoelectronic Technology, Beijing Jiaotong University, Beijing 100044, China*

[2]*Department of Physics and Astronomy, The University of Kansas, Lawrence, Kansas 66045, USA*

**jqhe@bjtu.edu.cn*

**yshwang@bjtu.edu.cn*

Abstract: We fabricated a van der Waals heterostructure by stacking together monolayers of MoS_2 and $ReSe_2$. Transient absorption measurements were performed to study the dynamics of charge transfer, indirect exciton formation, and indirect exciton recombination. The results show that the heterostructure form a type-II band alignment with the conduction band minimum and valance band maximum located in the MoS_2 and $ReSe_2$ layers, respectively. By using different pump-probe configurations, we found that electrons could efficiently transfer from $ReSe_2$ to MoS_2 and holes along the opposite direction. Once transferred, the electrons and holes form spatially indirect excitons, which have longer recombination lifetimes than excitons in individual monolayers. These results provide useful information for developing van der Waals heterostructure involving $ReSe_2$ for novel electronic and optoelectronic applications.

1. Introduction

The discovery of graphene in 2004 [1] has stimulated intensive research on a broad range of two-dimensional (2D) materials, among which layered transition metal dichalcogenides (TMDs) have attracted much attention. Most monolayer TMDs studied so far has a direct bandgap and thickness-dependent bandgaps. Their ultrathin thickness and superior electronic and optical properties make them promising materials for optoelectronic and electronic devices such as photodetectors [2-4], solar cells [5-7] and integrated circuits [8-10].

Among the semiconductors in the family of TMDs, MoS_2 has attracted the most attention. Bulk MoS_2 exhibits an indirect bandgap of about 1.2 eV, while its monolayer form is direct-gap semiconductor with a bandgap of about 1.8 eV [11, 12]. $ReSe_2$ is another representative semiconducting TMDs. Theoretical calculations showed that $ReSe_2$ lacks the indirect-to-direct bandgap transition often observed in TMDs [13-16]. It remains an indirect semiconductor from bulk to monolayer forms. Optical spectroscopic measurements indicated that its bandgap increases from 1.26 eV in the bulk to 1.32 eV in the monolayer at 80 K [13]. Monolayer layer $ReSe_2$ transistors have been fabricated, with high mobility and high photoresponsivity[15]. The excitons are strongly polarized with dipole vectors along different crystal directions, which persist from bulk down to monolayer thickness, as shown by polarization-resolved photoluminescence and transmission spectroscopy [17]. Unlike most TMDs with the 2H lattice structure

(such as MoS_2, $MoSe_2$, WS_2, and WSe_2), $ReSe_2$ crystals exhibit a distorted 1*T* lattice structure [15]. Owing to this lattice structure, $ReSe_2$ exhibits strong in-plane anisotropic optical, electronic, and mechanical properties [18-21].

Another research topic of great current interests associated with 2D materials is to develop van der Waals heterostructures by stacking together different monolayers. Since the van der Waals interlayer coupling does not require lattice matching of the component materials, this approach can produce a vast number of new materials [22]. In order to harness desired properties, different combinations of 2D materials have been designed and fabricated to tune the electrical and optical properties of the materials [23-30]. So far, combinations of the most common TMDs materials, such as MoS_2, $MoSe_2$, WS_2, and WSe_2, have been the main focus. The charge transfer properties in these heterostructure have been studied by transient absorption measurements [31-34]. However, the charge transfer in heterostructure involving $ReSe_2$ has not been investigated so far.

In this work, we fabricated a van der Waals heterostructure by stacking together monolayers of MoS_2 and $ReSe_2$. Transient absorption measurements were performed to study the dynamics of charge transfer, indirect exciton formation, and indirect exciton recombination. We found evidence of the type-II nature of this heterostructure, which facilitates the transfer of electrons from $ReSe_2$ to MoS_2 and holes along the opposite direction. When transferred, electrons and holes form spatially indirect excitons with longer recombination lifetimes than the excitons in individual monolayers. These results provide useful information for developing van der Waals heterostructures using $ReSe_2$.

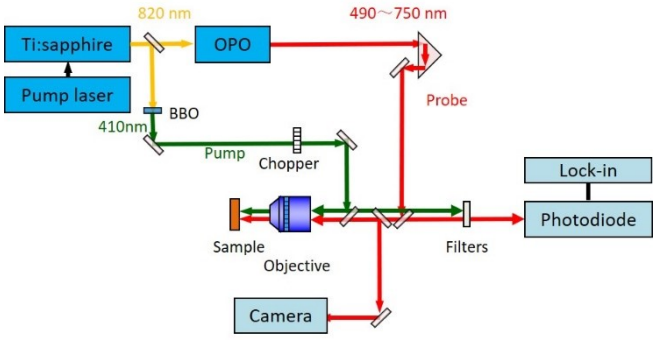

Fig. 1 Schematics of the differential reflection setup.

2. Experimental

Monolayer $ReSe_2$ films were acquired from 6 Carbon Technology Corporation. The films were fabricated by chemical vapor deposition (CVD) and then transferred to a silicon substrate, which is covered by a 300-nm thermally grown SiO_2 layer. Two monolayer MoS_2 flakes were obtained by micromechanical exfoliation of a bulk crystal onto polydimethylsiloxane (PDMS) substrates using adhesive tapes. One of them was transferred onto the $ReSe_2$ film, another onto another Si/SiO_2 substrate. The samples were annealed at 200 °C for 2 h in an Ar environment at a base pressure of about 5 Torr. Because the $ReSe_2$ is a polycrystalline film, the relative crystalline orientation between MoS_2 and $ReSe_2$ is unknown.

The photocarrier dynamics in the MoS_2-$ReSe_2$ heterostructure and the monolayers of MoS_2 and $ReSe_2$ was studied by a transient absorption technique [35]. Fig. 1 shows schematically the differential reflection setup used in this study. An 80-MHz mode-locked Ti:sapphire laser generates 100 fs pulses with a central wavelength of 820 nm. This pulse was divided to two parts by a beamsplitter. One part was used to pump an optical parametric oscillator to generate a signal output with a central wavelength in the range of 490-750 nm. The other part was used directly or focused to a beta barium borate crystal to generate its second harmonic at 410 nm. Different combinations of these three pulses were used as pump and probe pulses according to the measurement goals. The pump and probe beams were combined with a beamsplitter and focused to the sample surface through a microscope objective lens. The reflected beam was detected by a silicon photodiode. Color filters were used to prevent the unwanted light from reaching the photodiode. A lock-in amplifier was used to measure the voltage output of the photodiode. A mechanical chopper was placed at the pump path to modulate its intensity at 2 KHz. The voltage detected by the lock-in amplifier synchronized to the chopper is proportional to the differential reflection of the probe, $\Delta R/R_0 = (R-R_0)/R_0$, where R and R_0 are the reflection coefficients of the sample at the probe wavelength with the pump presence and without it, respectively. The differential reflection was measured as a function of the probe delay, which is defined as the difference of the arrival times of the probe and pump pulses at the sample. This was achieved by controlling the path length of the pump pulse with a linear motor stage. All the measurements were performed with the samples under ambient condition.

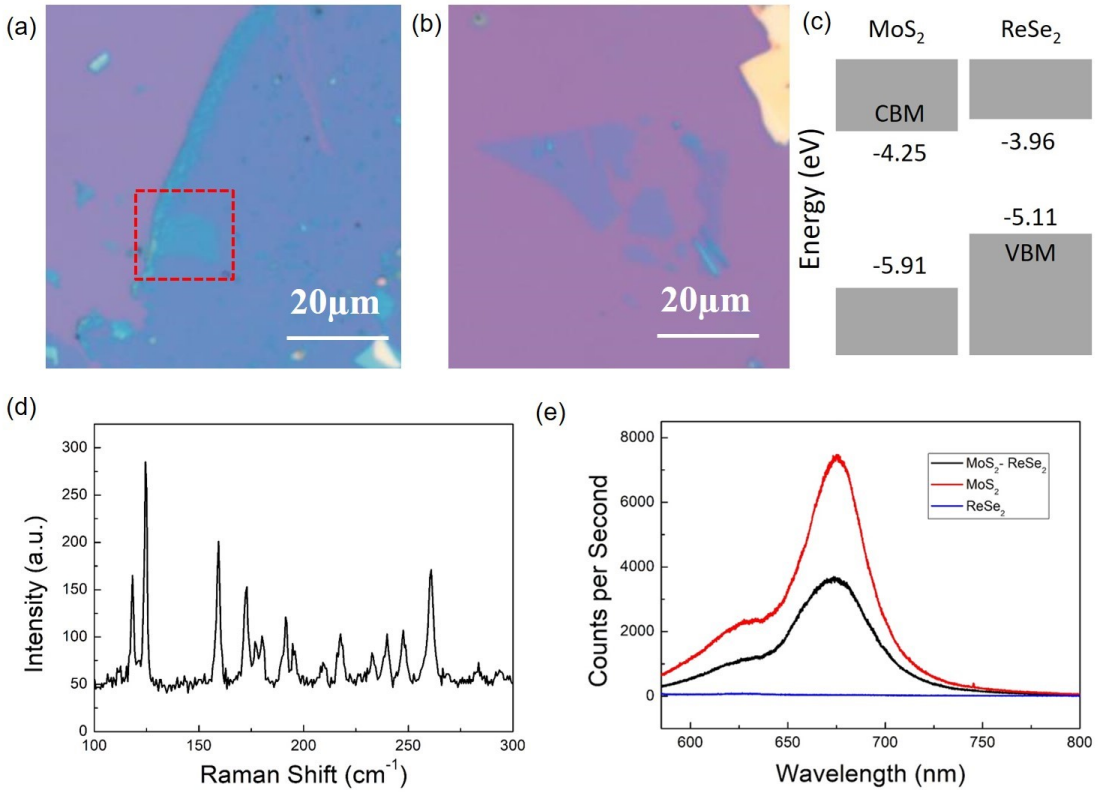

Fig. 2 (a) Optical microscope image of the $ReSe_2$ film and MoS_2-$ReSe_2$ heterostructure, the heterostructure is in the red dashed box. (b) Optical microscope image of the monolayer MoS_2 flake. (c) The predicted band alignment of the MoS_2-$ReSe_2$ heterostructure. The numbers are the energy differences from the vacuum level (in electron volts) according to the calculation. (d) Photoluminescence spectra of the samples.

3. Results and discussion

Figure 2(a) shows an optical microscope image of the monolayer $ReSe_2$ film and the MoS_2-$ReSe_2$ heterostructure on a Si/SiO_2 substrate. The other monolayer MoS_2 flake on a separated substrate is shown in Fig. 2(b). According to the predicted band alignment of this heterostructure [36], as shown in Fig. 2(c), MoS_2 and $ReSe_2$ form a type-II band alignment with the conduction band minimum (CBM) and valance band maximum (VBM) located in the MoS_2 and $ReSe_2$ layers, respectively. Note that in this calculation [36] the interlayer coupling was not included. The band alignment was determined directly from the electron affinity and ionization potential of individual monolayers of MoS_2 and $ReSe_2$ (which are labeled in the figure in the unit of eV). Due to this limitation, no values of the band offset are adopted. Figure 2(d) shows the Raman spectrum of the monolayers $ReSe_2$ film. The monolayer $ReSe_2$ have 18 potential Raman modes due to the presence of 12 atoms in each unit cell of the $ReSe_2$ crystal lattice [14]. There more than 10 distinctive Raman peaks have been detected in the Raman spectrum of monolayer $ReSe_2$ film. Raman peak at 125 cm^{-1} is observed and assigned to the E_g-like, as the vibration is mostly in-plane and symmetric [13]. The peaks located at 160 and 173 cm^{-1} are ascribed as A_g-like modes since the main vibrations are in the one-dimensional vertical direction [13].

Figure 2(e) shows the photoluminescence (PL) spectra measured from the MoS_2, $ReSe_2$, and the MoS_2-$ReSe_2$ heterostructure regions under the excitation of a 532-nm continuous-wave laser. The PL yield and the spectral shape of MoS_2 are both consistent with previously reported results of monolayer MoS_2 [37]. With the same experimental conditions, $ReSe_2$ film shows no detectable PL in this spectral range. For the heterostructure region, the PL peak position is close to that of MoS_2. This suggests that the optical bandgap of the MoS_2 layer is almost unchanged in the heterostructure. The peak height of the heterostructure is about 50% of that of the individual MoS_2 monolayer. This quenching of the MoS_2 peak is indicative of charge or energy transfer from MoS_2 to $ReSe_2$. The small quenching factor is consistent with results from other heterostructures involving MoS_2 [32], and can be attributed to the short exciton lifetime in this material. We also note that the PL from the heterostructure is slightly broader than monolayer MoS_2, which could be due to additional scattering of excitons introduced by defects in $ReSe_2$. However, more studies are needed to fully understand this feature.

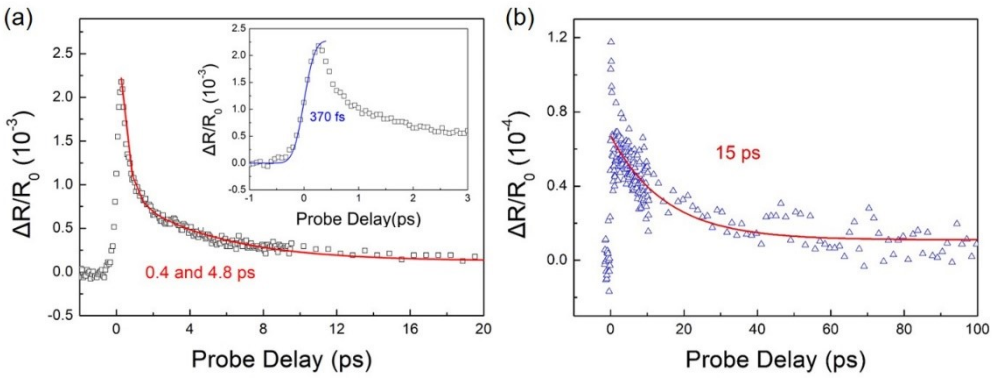

Fig. 3 Photocarrier dynamics in individual monolayers. (a) Differential reflection signal of monolayer MoS_2 measured with a 410 nm pump and a 672 nm probe pulses. The red line is a fit by a bi-exponential function. The inset provides a closer look at the data near zero probe delay. (b) Differential reflection signals of

monolayer $ReSe_2$ measured with a 672 nm pump and an 820 nm probe pulses. The red line is a fit by an exponential function.

In the transient absorption measurements, we first investigated the individual monolayers of MoS_2 and $ReSe_2$ samples. Figure 3(a) shows the differential reflection signal of MoS_2. In this measurement, a 410 nm pump pulse with a fluence of 5.6 μJ cm^{-2} was used to inject photocarriers in the sample. A 672 nm probe pulse was used to study their temporal dynamics. The rise of the signal can be fit by the integral of a Gaussian function with a full width at half maximum of 370 fs, as indicated by the blue curve over the data points in the inset of Fig. 3(a). The decay of the signal can be fit by a bi-exponential function, as indicated by the red line in Fig. 3(a), with a short and long time constant of about 0.4 and 4.8 ps, respectively. By repeating the measurement with other pump fluences, we found that the decay time constants are independent of the pump fluence while the magnitude increases linearly with the fluence. The short time constant can be attributed to the exciton formation process, based on previous studies [38, 39]. The long time constant reflects the recombination lifetime of the excitons [35]. This relatively short lifetime is controlled by nonradiative recombination of excitons. Figure 3(b) shows the differential reflection signal from the monolayer $ReSe_2$. A 672 nm pulses with a peak fluence of 76 μJ cm^{-2} and an 820 nm pulses were used as the pump and probe, respectively. The decay of the signal can be fit by a single exponential function, as indicated by the red line, with a time constant of about 15 ps. Similarly, this time constant is attributed to the nonradiative recombination lifetime in $ReSe_2$. We note that due to the relatively low signal-to-noise ratio of $ReSe_2$, no multiple exponential fits were attempt.

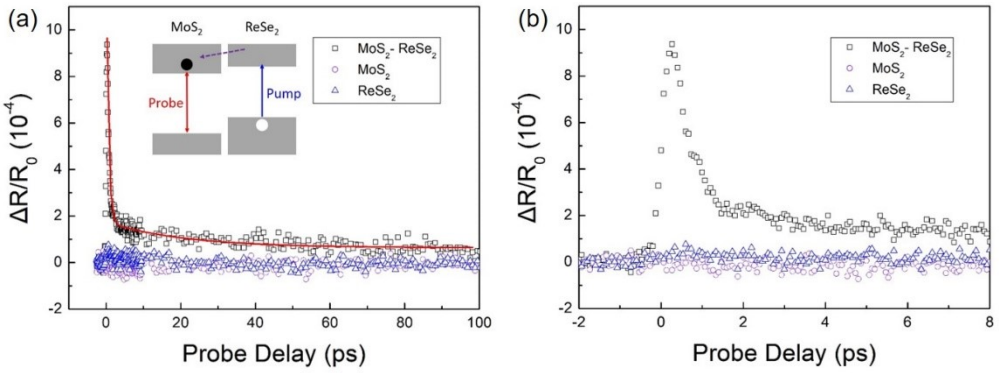

Fig. 4 Electron transfer from $ReSe_2$ to MoS_2. (a) Black squares show the differential reflection signal from the MoS_2-ReS_2 heterostructure sample with an 820 nm pump and a 672 nm probe pulses. The red line is a fit. The purple circles and the blue triangles are signals from the MoS_2 and ReS_2 monolayer samples under the same conditions, respectively, showing lack of signal from these samples, as expected. (b) Same as (a) but over a shorter time range to show the initial dynamics.

Next, we performed transient absorption measurements with different pump-probe configurations to study the MoS_2-$ReSe_2$ heterostructure. We first studied the electron transfer from $ReSe_2$ to MoS_2, with a pump-probe configuration shown in the inset of Fig. 4(a). We selectively excite electrons in $ReSe_2$ with an 820 nm pump pulse (blue vertical arrow). The pump photon energy is not enough to excite the MoS_2 layer, which has an optical bandgap of 1.85 eV. After been excited, the electrons in $ReSe_2$ are expected

to transfer to MoS_2 across the van der Waals interface (violet dashed arrow). A 672 nm probe pulse is tuned to the optical bandgap of the MoS_2 to monitor the electron transfer process (red vertical arrow). The black symbols in Figs. 4(a) and 4(b) show the obtained signal on long and short time ranges, respectively, with a pump pulse fluence of 22 μJ cm^{-2}. For comparison, no signal was observed from the two monolayer samples, as shown by the purple circles and blue triangles. The lack of signal from these two samples are expected: For MoS_2, the pump pulse has no sufficient energy to excite carriers, while for $ReSe_2$, the probe photon energy is too high compared to its bandgap to effectively detect carriers. Hence, the signal from the heterostructure can only be attributed to the electrons that are excited in $ReSe_2$ and sequentially transferred to MoS_2. We found that the signal reaches a peak on an ultrashort time scale, which is limited by the time resolution of this measurement. This indicates that the electron transfer is a sub-100 fs process. The decay of the signal can be fit by bi-exponential function, as indicated by the red line in Fig. 4(a), with the short and long time constants of about 0.5 and 21 ps, respectively. The long time constant reflects that the lifetime of the transferred electrons in MoS_2 is about 4 times longer than the exciton lifetime in monolayer MoS_2, due to the charge separation: Since electrons and holes populate the MoS_2 and $ReSe_2$ layers, respectively, their recombination is suppressed. The short time constant could be attributed to the formation of indirect exciton of electrons in MoS_2 and holes in $ReSe_2$.

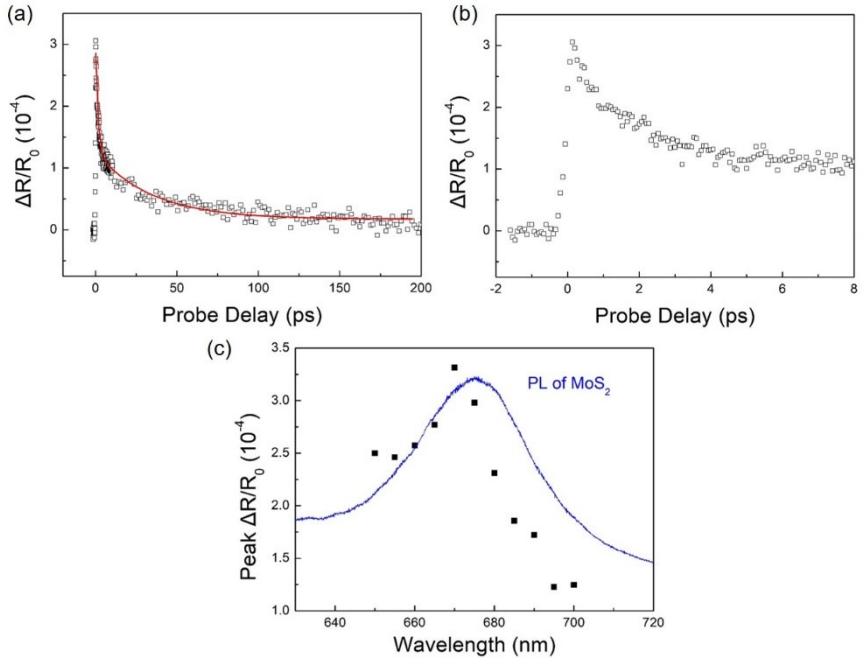

Fig. 5 Hole transfer from MoS_2 to $ReSe_2$. (a) Differential reflection signals of the heterostructure sample measured with a 672 nm pump and an 820 nm probe pulses. The red line is a fit by an exponential function. (b) The same as (a) but in a shorter time range. (c) Peak differential reflection signal from the heterostructure as a function of the pump wavelength (black squares) and the PL spectrum of the MoS_2 (blue curve).

Since the bandgap of ReS_2 is smaller than MoS_2, the observation of electron transfer from ReS_2 to MoS_2 indicates the band alignment is type-II, with the CBM and VBM located in the MoS_2 and ReS_2 layers, respectively, which is consistent with theory. Such an alignment should allow transfer of holes from MoS_2 to ReS_2. To observe this process, we excite the heterostructure sample with a 76 μJ cm^{-2} and

672-nm pump pulse, and probe the ReS_2 layer of the heterostructure with an 820-nm probe. Figures 5(a) and 5(b) show the differential reflection signal in long and short time ranges, respectively. Since the experimental conditions are identical to the measurement of the individual ReS_2 monolayer, as shown in Fig. 3(b), the two samples can be directly compared. We find that the signal from the heterostructure is about 3 times higher than the monolayer ReS_2. For the MoS_2-$ReSe_2$ heterostructure, the pump excites electrons and holes in both layers. Since electrons excited in ReS_2 transfer to MoS_2, if holes do not transfer from MoS_2 to ReS_2, the carrier population in ReS_2 of the heterostructure would be lower than that of the individual ReS_2, and hence the signal would be smaller. Therefore, the observed increase of the signal in the heterostructure shows that holes can transfer from MoS_2 to ReS_2. The decay of the signal from the heterostructure can be fit by a bi-exponential function, as indicated by the red line in Fig. 5(a), with time constants of about 1.5 and 34 ps, respectively. The short time constant could be associated with cooling of hot holes. Note that in this measurement the probe is not tuned to the excitonic resonance of $ReSe_2$, and hence is not expected to be sensitive to the exciton formation process. However, since holes transfer to $ReSe_2$ with large energy, their energy relaxation from the states being probed to the top of the valence band causes a decrease of the signal. The long time constant reflects the lifetime of the carriers, which is about twice longer than of individual monolayer $ReSe_2$. Similarly, the extended lifetime can be attributed to the separation of electrons and holes due to charge transfer.

In this configuration to study hole transfer, we intend to excite MoS_2 with the 670-nm pump. However, since ReS_2 has a smaller bandgap, the pump also excites ReS_2. Therefore, the 820-nm probe senses holes that could be either injected directly in ReS_2 or transferred from MoS_2. To separate the two contributions, and thus further confirm existence of hole transfer, we studied how the signal changes when we tune the pump wavelength around the optical bandgap of MoS_2. The results are plotted in Fig. 5(c) along with the PL spectrum of MoS_2 for comparison. The strong dependence shows clearly the important role of the transferred holes, since the carrier density excited in $ReSe_2$ is not expected to have a strong dependence on the pump wavelength in this small range. In particular, when the pump wavelength is significantly longer than the PL peak energy, the signal is about 1.2×10^{-4}. This can be viewed as the contribution from the holes excited in $ReSe_2$ since the MoS_2 is not excited. At shorter pump wavelengths that can excite MoS_2, the signal reaches to about 3×10^{-4}, due to the additional contribution to the hole population in ReS_2 from the transfer.

4. Conclusions

We have studied charge transfer in a van der Waals heterostructure composed of monolayers of MoS_2 and $ReSe_2$. Transient absorption measurements show strong evidence of ultrafast electron transfer from ReS_2 to MoS_2 and hole transfer from MoS_2 to ReS_2. These results show that the band alignment of this heterostructure is type-II with the conduction band minimum located in MoS_2 and valence band maximum in ReS_2. Separation of electrons and holes in different layers prolonged their recombination lifetime. These results introduce $ReSe_2$ as a new building block to construct van der Waals heterostructure with good charge transfer properties, which can be used in electronic and optoelectronic devices.

Funding

We are grateful for the financial support of the National Key R&D Program of China (2016YFA0202302), the National Natural Science Foundation of China (61527817, 61875236), Initiative Postdocs Supporting Program of China (BX201600013), General Financial Grant from the China Postdoctoral Science Foundation (2017M610756), Overseas Expertise Introduction Center for Discipline Innovation, 111 Center of China, and National Science Foundation of USA (DMR-1505852).

References

1. K. S. Novoselov, A. K. Geim, S. V. Morozov, D. Jiang, Y. Zhang, S. V. Dubonos, I. V. Grigorieva, and A. A. Firsov, "Electric field effect in atomically thin carbon films," Science **306**, 666-669 (2004).
2. Z. Yin, H. Li, H. Li, L. Jiang, Y. Shi, Y. Sun, G. Lu, Q. Zhang, X. Chen, and H. Zhang, "Single-layer MoS_2 phototransistors," ACS Nano **6**, 74-80 (2012).
3. S. M. Cui, H. H. Pu, S. A. Wells, Z. H. Wen, S. Mao, J. B. Chang, M. C. Hersam, and J. H. Chen, "Ultrahigh sensitivity and layer-dependent sensing performance of phosphorene-based gas sensors," Nat. Commun. **6** 8632 (2015).
4. O. Lopez-Sanchez, D. Lembke, M. Kayci, A. Radenovic, and A. Kis, "Ultrasensitive photodetectors based on monolayer MoS_2," Nat. Nanotechnol. **8**, 497-501 (2013).
5. M. L. Tsai, S. H. Su, J. K. Chang, D. S. Tsai, C. H. Chen, C. I. Wu, L. J. Li, L. J. Chen, and J. H. He, "Monolayer MoS_2 heterojunction solar cells," ACS Nano **8**, 8317-8322 (2014).
6. J. M. Yun, Y. J. Noh, C. H. Lee, S. I. Na, S. Lee, S. M. Jo, H. I. Joh, and D. Y. Kim, "Exfoliated and partially oxidized MoS_2 nanosheets by one-pot reaction for efficient and stable organic solar cells," Small **10**, 2319-2324 (2014).
7. E. Gourmelon, O. Lignier, H. Hadouda, G. Couturier, J. C. Bernede, J. Tedd, J. Pouzet, and J. Salardenne, "MS_2 (M=W, Mo) photosensitive thin films for solar cells," Sol. Energy Mater. Sol. Cells **46**, 115-121 (1997).
8. B. Radisavljevic, M. B. Whitwick, and A. Kis, "Integrated circuits and logic operations based on single-layer MoS_2," ACS Nano **5**, 9934-9938 (2011).
9. B. W. H. Baugher, H. O. H. Churchill, Y. Yang, and P. Jarillo-Herrero, "Optoelectronic devices based on electrically tunable p-n diodes in a monolayer dichalcogenide," Nat. Nanotechnol. **9**, 262-267 (2014).
10. R. Cheng, S. Jiang, Y. Chen, Y. Liu, N. Weiss, H. C. Cheng, H. Wu, Y. Huang, and X. Duan, "Few-layer molybdenum disulfide transistors and circuits for high-speed flexible electronics," Nat. Commun. **5**, 5143 (2014).
11. K. K. Kam and B. A. Parkinson, "Detailed photocurrent spectroscopy of the semiconducting group-Vi transition-metal dichalcogenides," J. Phys. Chem. **86**, 463-467 (1982).
12. K. F. Mak, C. Lee, J. Hone, J. Shan, and T. F. Heinz, "Atomically thin MoS_2: a new direct-gap semiconductor," Phys. Rev. Lett. **105** 136805 (2010).
13. H. Zhao, J. B. Wu, H. X. Zhong, Q. S. Guo, X. M. Wang, F. N. Xia, L. Yang, P. H. Tan, and H. Wang, "Interlayer interactions in anisotropic atomically thin rhenium diselenide," Nano Res. **8**, 3651-3661 (2015).
14. D. Wolverson, S. Crampin, A. S. Kazemi, A. Ilie, and S. J. Bending, "Raman spectra of monolayer, few-Layer, and bulk $ReSe_2$: an anisotropic layered semiconductor," ACS Nano **8**, 11154-11164 (2014).
15. S. Yang, S. Tongay, Y. Li, Q. Yue, J. B. Xia, S. S. Li, J. Li, and S. H. Wei, "Layer-dependent electrical and optoelectronic responses of $ReSe_2$ nanosheet transistors," Nanoscale **6**, 7226-7231 (2014).
16. A. L. Elias, N. Perea-Lopez, A. Castro-Beltran, A. Berkdemir, R. T. Lv, S. M. Feng, A. D. Long, T. Hayashi, Y. A. Kim, M. Endo, H. R. Gutierrez, N. R. Pradhan, L. Balicas, T. E. Mallouk, F. Lopez-Urias, H. Terrones, and M. Terrones, "Controlled synthesis and transfer of large-Area WS_2 sheets: from single layer to few Layers," ACS Nano **7**, 5235-5242 (2013).
17. A. Arora, J. Noky, M. Druppel, B. Jariwala, T. Deilmann, R. Schneider, R. Schmidt, O. Del Pozo-Zamudio, T. Stiehm, A. Bhattacharya, P. Kruger, S. Michaelis de Vasconcellos, M. Rohlfing, and R. Bratschitsch, "Highly anisotropic in-

plane excitons in atomically thin and bulk like 1T'-$ReSe_2$," Nano Lett. **17**, 3202-3207 (2017).

18. S. X. Yang, C. Wang, H. Sahin, H. Chen, Y. Li, S. S. Li, A. Suslu, F. M. Peeters, Q. Liu, J. B. Li, and S. Tongay, "Tuning the optical, magnetic, and electrical properties of $ReSe_2$ by nanoscale strain engineering," Nano Lett. **15**, 1660-1666 (2015).
19. D. B. Seley, M. Nath, and B. A. Parkinson, "$ReSe_2$ nanotubes synthesized from sacrificial templates," J. Mater. Chem. **19**, 1532-1534 (2009).
20. K. Friemelt, M. C. Luxsteiner, and E. Bucher, "Optical properties of the layered transition-metal-dichalcogenide ReS_2: anisotropy in the van der Waals plane," J. Appl. Phys. **74**, 5266-5268 (1993).
21. C. H. Ho and C. E. Huang, "Optical property of the near band-edge transitions in rhenium disulfide and diselenide," J. Alloys Compd. **383**, 74-79 (2004).
22. A. K. Geim and I. V. Grigorieva, "Van der Waals heterostructures," Nature **499**, 419-425 (2013).
23. Y. Liu, N. O. Weiss, X. Duan, H. Cheng, Y. Huang, and X. Duan, "Van der Waals heterostructures and devices," Nat. Rev. Mater. **1**, 16042 (2016).
24. K. S. Novoselov, A. Mishchenko, A. Carvalho, and A. H. Castro Neto, "2D materials and van der Waals heterostructures," Science **353** aac9439 (2016).
25. P. Rivera, J. R. Schaibley, A. M. Jones, J. S. Ross, S. Wu, G. Aivazian, P. Klement, K. Seyler, G. Clark, N. J. Ghimire, J. Yan, D. G. Mandrus, W. Yao, and X. Xu, "Observation of long-lived interlayer excitons in monolayer $MoSe_2$-WSe_2 heterostructures," Nat. Commun. **6**, 6242 (2015).
26. C. H. Lee, G. H. Lee, A. M. van der Zande, W. Chen, Y. Li, M. Han, X. Cui, G. Arefe, C. Nuckolls, T. F. Heinz, J. Guo, J. Hone, and P. Kim, "Atomically thin p-n junctions with van der Waals heterointerfaces," Nat. Nanotechnol. **9**, 676-681 (2014).
27. H. M. Hill, A. F. Rigosi, K. T. Rim, G. W. Flynn, and T. F. Heinz, "Band alignment in MoS_2/WS_2 transition metal dichalcogenide heterostructures probed by scanning tunneling microscopy and spectroscopy," Nano Lett. **16**, 4831-4837 (2016).
28. B. Miller, A. Steinhoff, B. Pano, J. Klein, F. Jahnke, A. Holleitner, and U. Wurstbauer, "Long-lived direct and indirect interlayer excitons in van der Waals heterostructures," Nano Lett. **17**, 5229 (2017).
29. J. S. Ross, P. Rivera, J. R. Schaibley, E. L. Wong, H. Yu, T. Taniguchi, K. Watanabe, J. Yan, D. Mandrus, and D. H. Cobden, "Interlayer exciton optoelectronics in a 2D heterostructure p-n junction," Nano Lett. **17**, 638-643 (2017).
30. K. L. Seyler, P. Rivera, H. Y. Yu, N. P. Wilson, E. L. Ray, D. G. Mandrus, J. Q. Yan, W. Yao, and X. D. Xu, "Signatures of moire-trapped valley excitons in $MoSe_2/WSe_2$ heterobilayers," Nature **567**, 66 (2018).
31. F. Ceballos, M. Z. Bellus, H. Y. Chiu, and H. Zhao, "Probing charge transfer excitons in a $MoSe_2$-WS_2 van der Waals heterostructure," Nanoscale **7**, 17523-17528 (2015).
32. F. Ceballos, M. Z. Bellus, H. Y. Chiu, and H. Zhao, "Ultrafast charge separation and indirect exciton formation in a MoS_2-$MoSe_2$ van der Waals heterostructure," ACS Nano **8**, 12717-12724 (2014).
33. X. Hong, J. Kim, S. F. Shi, Y. Zhang, C. Jin, Y. Sun, S. Tongay, J. Wu, Y. Zhang, and F. Wang, "Ultrafast charge transfer in atomically thin MoS_2/WS_2 heterostructures," Nat. Nanotechnol. **9**, 682-686 (2014).
34. K. Wang, B. Huang, M. Tian, F. Ceballos, M. W. Lin, M. Mahjouri-Samani, A. Boulesbaa, A. A. Puretzky, C. M. Rouleau, M. Yoon, H. Zhao, K. Xiao, G. Duscher, and D. B. Geohegan, "Interlayer coupling in twisted WSe_2/WS_2 bilayer heterostructures revealed by optical spectroscopy," ACS Nano **10**, 6612-6622 (2016).
35. F. Ceballos and H. Zhao, "Ultrafast laser spectroscopy of two-dimensional materials beyond graphene," Adv. Funct. Mater. **27**, 1604509 (2017).
36. M. Li, M. Z. Bellus, J. Dai, L. Ma, X. Li, H. Zhao, and X. C. Zeng, "A type-I van der Waals heterobilayer of $WSe_2/MoTe_2$," Nanotechnology **29**, 335203 (2018).
37. A. Splendiani, L. Sun, Y. Zhang, T. Li, J. Kim, C. Y. Chim, G. Galli, and F. Wang, "Emerging photoluminescence in

monolayer MoS_2," Nano Lett. **10**, 1271-1275 (2010).

38. F. Ceballos, Q. Cui, M. Z. Bellus, and H. Zhao, "Exciton formation in monolayer transition metal dichalcogenides," Nanoscale **8**, 11681-11688 (2016).

39. P. Steinleitner, P. Merkl, P. Nagler, J. Mornhinweg, C. Schuller, T. Korn, A. Chernikov, and R. Huber, "Direct observation of ultrafast exciton formation in a monolayer of WSe_2," Nano Lett. **17**, 1455-1460 (2017).